

Title: **Mechanical cell-substrate feedback explains pairwise and collective endothelial cell behavior in vitro**

Running title: **Modeling mechanical cell-ECM feedback**

René F. M. van Oers<sup>1,2,\*</sup>, Roeland M. H. Merks<sup>1,2,3,\*\*</sup>

**1** Life Sciences, Centrum Wiskunde & Informatica, Amsterdam, The Netherlands

**2** Netherlands Consortium for System Biology - Netherlands Institute for Systems Biology, Amsterdam, The Netherlands

**3** Mathematical Institute, Leiden University, Leiden, The Netherlands

\* Present address: Oral Cell Biology, Academic Centre for Dentistry Amsterdam (ACTA), The Netherlands

\*\* E-mail: roeland.merks@cwi.nl

**Keywords (6 max):** cell traction, angiogenesis, extracellular matrix, Cellular Potts model, finite-element method, mechanical cell-cell communication

## Abstract

In vitro cultures of endothelial cells are a widely used model system of the collective behavior of endothelial cells during vasculogenesis and angiogenesis. When seeded in a extracellular matrix, endothelial cells can form blood vessel-like structures, including vascular networks and sprouts. Endothelial morphogenesis depends on a large number of chemical and mechanical factors, including the compliancy of the extracellular matrix, the available growth factors, the adhesion of cells to the extracellular matrix, cell-cell signaling, etc. Although various computational models have been proposed to explain the role of each of these biochemical and biomechanical effects, the mechanisms underlying in vitro angiogenesis are still poorly understood. Most explanations focus on predicting the whole vascular network or sprout from the underlying cell behavior, and ignore the intermediate organizational levels of the system. Here we show, using a hybrid

Cellular Potts and finite-element computational model, that a single set of biologically plausible rules describing (a) the contractile forces that endothelial cells exert on the ECM, (b) the resulting strains in the extracellular matrix, and (c) the cellular response to the strains, suffices for reproducing the behavior of individual endothelial cells and the interactions of endothelial cell pairs in compliant matrices. With the same set of rules, the model also reproduces network formation and sprouting from epithelial spheroids. Combining the present, mechanical model with aspects of previously proposed mechanical and chemical models may lead to a more complete understanding of *in vitro* angiogenesis.

## Introduction

How the behavior of the cells in a multicellular organism is coordinated to form structured tissues, organs and whole organisms, is a central question in developmental biology. Keys to answering this question are chemical and mechanical cell-cell communication and the biophysics of self-organization. Cells exchange information by means of diffusing molecular signals, and by membrane-bound molecular signals for which direct cell-cell contact is required. In general, these developmental signals are short-lived and move over short distances. The extracellular matrix (ECM), the jelly or hard materials that cells secrete, provides the micro-environment the cells live in. Apart from its supportive function, the ECM mediates molecular (1) and biomechanical (2) signals between cells. Mechanical signals, in the form of tissue strains and stresses to which cells respond (3), can act over long distances and integrate mechanical information over the whole tissue (4), and also mediate short-range, mechanical cell-cell communication (2). How such mechanical cell-cell communication via the ECM can coordinate the self-organization of cells into tissues is still poorly understood. Here we propose a cell-based model of endothelial cell motility on compliant matrices to address this problem.

A widely used approach to study the role of cell-ECM interactions in coordinating collective cell behavior is to isolate cells and the ECM (potentially from an exogenous source) in a cell culture. This makes it possible to study the intrinsic ability of cells to form tissues in absence

of potential organizing signals or pre-patterns from adjacent tissues. A problem particularly well-studied in cell cultures is the ability of endothelial cells to form blood vessel like structures, including the formation of vascular-like networks from dispersed cells and the sprouting of spheroids. To this end, endothelial cells are seeded on top of an ECM material (e.g. Matrigel, collagen, or fibrin) in dispersed, initial configurations (5, 6), as cellular spheroids embedded in the ECM (7, 8), or as confluent monolayers (9, 10, 11). Although the conditions required for vascular-like development in these in vitro culture systems are well established, the mechanisms driving pattern formation of endothelial cells are heavily debated, and a wide range of plausible mechanisms has been proposed in the form of mathematical and computational models reproducing aspects of angiogenesis (reviewed in (12, 13, 14)).

Typical ingredients of network formation models are (a) an attractive force between endothelial cells, which is (b) proportional to the cell density, and (c) inhibited or attenuated at higher cellular densities. The attractive force can be due to mechanical traction or due to chemotaxis. For example, Manoussaki and coworkers (15, 16) proposed a mechanical model in which endothelial cells exert a uniform traction force on the ECM, dragging the ECM and the associated endothelial cell towards them. The traction forces saturated at a maximum cell density. Namy and coworkers(17) replaced the endothelial cells' passive motion along with the ECM for active cell motility via haptotaxis, in which cells move actively towards higher concentrations of the ECM. Both models also included a strain-biased random walk term for the endothelial cells, but they found that it had little effect on network formation; the mechanism was dominated by cell aggregation. In their model based on chemotaxis, Preziosi and coworkers (18, 19) assumed that cells attract one another via the secreted chemoattractant VEGF. Due to diffusion and first-order degradation, the chemoattractant forms exponential gradients around cells leading to cell aggregation in much the same way as that assumed in the Manoussaki and Namy models. These chemotaxis-based hypotheses formed the basis for a series of cell-based models based on the cellular Potts model. Assuming chemotactic cell-cell attraction, and a biologically-plausible overdamped cell motility, the cells in these CPM models form round aggregates, in accordance

with the Keller-Segel model of cell aggregation (20). Additional assumptions, including an elongated cell shape (21) or contact inhibition of chemotaxis (22) are needed to transform these circular aggregates into vascular-like network patterns. Related network formation models studied the role of ECM-bound growth factors (23, 24) and a range of additional secreted and exogenous growth factors (24), and studied the ability of the contact-inhibition mechanism to produce three-dimensional blood-vessel-like structures (25), Szabó and coworkers found that in culture, astroglia-related rat C6 cells and muscle-related mouse C2C12 cells organize into network-like structures on rigid culture substrates (26), such that ECM-density or chemoattractant gradients are excluded. They proposed a model where cells were preferentially attracted to or preferentially adhered to locally elongated structures. An alternative mechanism for “gel-free” network formation was found in the cell elongation mechanism (21) that also produces networks in absence of chemoattractant gradients (27).

Paradoxically, despite the diverse assumptions underlying the mathematical models proposed for vascular network formation, many are at least partly supported by experimental evidence. This suggests that a combination of chemotaxis, and chemical and mechanical cell-ECM interactions drives network formation, or that each alternative mechanism operates in a different tissue, developmental stage, or culture condition. A problem is that one mathematical representation may represent a range of equivalent alternative underlying mechanisms. For example, a model representing cell-cell attraction cannot distinguish between chemotaxis-based cellular attraction (18, 19, 21, 22), attraction via haptotaxis (17), direct mechanical attraction (28, 15) or cell shape dependent adhesion (26, 29), because the basic principles underlying these models are equivalent (22, 12). As a solution to this problem, a sufficiently correct complete description of endothelial cell behavior should suffice for the emergence of the subsequent levels of organization of the system, an approach that requires that the system has been experimentally characterized at all levels of organization. The role of cell traction and ECM mechanics during *in vitro* angiogenesis have been characterized experimentally particularly well, making it a good starting point for such a multiscale approach. Endothelial cells apply traction forces on the extracellular

matrix, as demonstrated by a variety of techniques, e.g., wrinkle formation on elastic substrates (9), force-generation on micropillar substrates (30) and traction force microscopy (31, 6). Using scanning electron microscopy, Vernon and Sage (9) found that ECM fibers radiate from endothelial cells cultured in Matrigel, suggesting that the traction forces reorient the fiber orientation in the extracellular matrix. The cellular traction forces produce local strains in the matrix, which can affect the motility of nearby cells (2). Thus endothelial cells can both generate, and respond to local strains in the extracellular matrix, suggesting a feedback loop that may act as a channel for mechanical cell-cell communication (2) and hence coordinate collective cell behavior. Here, we use a hybrid cellular Potts and finite-element model to show that a set of simple assumptions mimicking mechanical cell-cell communication via the ECM suffices to reproduce observed single cell behavior (32, 33), pairwise cell interactions (2) and network formation and sprouting .

## Mathematical Model

To model the biomechanical interactions between endothelial cells and compliant matrices, we developed a hybrid of the Cellular Potts model (CPM) (34, 35) to represent the stochastic motility of the endothelial cells, and a finite-element model (FEM) (36, 37, 38) of the compliant extracellular matrix. A documented simulation code is provided as part of the Supporting Material (supporting text and Code S1) and a detailed list of parameter values is given in Table S1.

### Cellular Potts model

We used the cellular Potts model (CPM) (34, 35) to mimic the random motility of cells. The CPM represents cells on a regular square lattice, with one biological cell covering a cluster of connected lattice sites. To mimic random cell motility, the CPM iteratively expands and retracts the boundaries of the cells, depending on the forces acting on them and on the forces exerted by the cells themselves, which are summarized in a balance of forces represented by the Hamiltonian,

$$H = \sum_{s \in \text{cells}} \lambda \left( \frac{a(s) - A(s)}{A(s)} \right)^2 + \sum_{(\vec{x}, \vec{x}')} J(s(\vec{x}), s(\vec{x}')) (1 - \delta(s(\vec{x}), s(\vec{x}'))). \quad (1)$$

The first term is an (approximate) volume constraint, with  $a(s)$  the actual volume of the cells,  $A(s)$ , a resting volume, and  $\lambda$  an elasticity parameter that regulates the permitted fluctuation around the resting volume. The second term represents cell-cell and cell-medium adhesion, where  $J(s(\vec{x}), s(\vec{x}'))$  is the contact cost between two neighboring pixels. Throughout the manuscript we use neutral cell-cell adhesion settings for which cells do not adhere  $J(s(\vec{x}), s(\vec{x}')) = 2.5$  at cell-cell interfaces, and  $J(s(\vec{x}), 0) = J(0, s(\vec{x}')) = 1.25$  at cell-medium interfaces, with  $s(\vec{x}) > 0$  and  $s(\vec{x}') > 0$ .

The CPM iteratively selects a random lattice site  $\vec{x}'$  and attempts to copy its state,  $s(\vec{x}')$ , into a randomly selected adjacent lattice site  $\vec{x}$ . To reflect the physical, “passive” responses of the cells to forces acting on it, the copy step is always accepted if it minimizes the Hamiltonian. To mimic the active motility of biological cells, which potentially counteracts forces from neighboring cells, we accept the moves with Boltzmann probability if they increase the Hamiltonian,

$$P(\Delta H) = \begin{cases} 1 & \text{if } \Delta H < 0 \\ e^{-\Delta H/T} & \text{if } \Delta H \leq 0. \end{cases} \quad (2)$$

where  $\Delta H$  is the change in H if the copying were to occur, and  $T > 0$  parameterizes the intrinsic cell motility.

During one Monte Carlo Step (MCS), we perform  $n$  such copy attempts, with  $n$  equal to the number of sites in the lattice. To prevent cells from splitting up, we apply a connectivity constraint that rejects moves that would split a cell (21).

## Finite Element Model of substrate

A two-dimensional finite element model (FEM; reviewed in (36, 37, 38)) is used to describe the compliant substrate on the which cells move. The FEM represents the substrate as a lattice of

elastic finite elements,  $e$ , with each element corresponding to a pixel of the CPM. The nodes of the elements interact with each other via the set of equations,

$$\underline{\underline{K}}\underline{u} = \underline{f}, \quad (3)$$

with stiffness matrix  $\underline{\underline{K}}$ , displacement  $\underline{u}$ , and forces  $\underline{f}$ .  $\underline{u}$  contains the displacements of all nodes, which are the unknowns that the FEM calculates based on the traction forces  $\underline{f}$  that the cells apply onto the ECM. In a two-dimensional analysis the forces  $\underline{f}$  are divided by the thickness they are working on. For this we assume an effective substrate thickness  $t = 10 \mu m$

To a first approximation, in this work we consider an isotropic, uniform, linearly elastic substrate (39, 40). The global stiffness matrix  $\underline{\underline{K}}$  is assembled from the element stiffness matrices  $\underline{\underline{K}}_e$ . The element stiffness matrices describe the interactions of the nodes of each element,  $e$ , with one another,

$$\underline{\underline{K}}_e = \int_{\Omega} \underline{\underline{B}}^T \underline{\underline{D}} \underline{\underline{B}} d\Omega. \quad (4)$$

where  $\underline{\underline{B}}$ —the conventional strain-displacement matrix for a four-noded quadrilateral element—relates the node displacements  $\underline{u}_e$  to the local strains, as,

$$\underline{\epsilon} = \underline{\underline{B}}\underline{u}_e. \quad (5)$$

$\underline{\underline{D}}$  is the material property matrix. Assuming plane stress conditions,

$$\underline{\underline{D}} = \frac{E}{1 - \nu^2} \begin{pmatrix} 1 & \nu & 0 \\ \nu & 1 & 0 \\ 0 & 0 & \frac{1}{2}(1 - \nu) \end{pmatrix} \quad (6)$$

where  $E$  is the material's Young's modulus, and  $\nu$  is Poisson's ratio. Throughout this study, we use a Poisson's ratio  $\nu$  of 0.45 and stiffness values  $E$  ranging from 0.5kPa to 32kPa, which are plausible values for most cell culture substrates (41, 42, 40).

## Mechanical cell-substrate coupling

To simulate cell-substrate feedback we alternate the Cellular Potts steps with finite element iterations. We assume that cells apply a cell-shape dependent traction on the ECM and the cells respond to the resulting ECM strains by adjusting their cell shape. Using the CPM grid as the finite-element mesh, the pixels of the CPM become four-node square elements in the FE-mesh. Adopting the model by Lemmon & Romer (43), we assume that each node  $i$  covered by a CPM cell pulls on all other nodes  $j$  in the same cell, at a force proportional to distance  $\vec{d}_{i,j}$ . The resultant force  $\vec{F}_i$  on node  $i$  then becomes,

$$\vec{F}_i = \mu \sum_j \vec{d}_{i,j} (\Delta x)^4, \quad (7)$$

where  $\Delta x$  is the lattice spacing and  $\mu$  gives the tension per unit length. This parameter has been scaled such that the total cell traction corresponds to experimentally reported values (44). We used a value of  $\mu = 0.01nN/\mu m$  throughout the simulations. The factor  $\Delta x^4$  reflects the fact that a change in element size changes the area for node  $i$  and the number of nodes  $j$  pulling at node  $i$ . The resultant forces point towards the cell centroid, and are proportional to the distance from it (Fig. 1). In this way a CPM configuration yields a traction force  $\underline{F}$ , which is added to the forces  $\underline{f}$  for the finite element calculation. To calculate the resulting ECM strains, we solve  $\underline{K}\underline{u} = \underline{f}$  for the node displacements  $\underline{u}$  with a preconditioned conjugate gradient (PCG) solver (45), and derive the local strains using Eq. 5.

After a steady-state solution for the finite-element model has been obtained, we run a Monte Carlo Step of the CPM. We assume durotaxis, i.e., the CPM cells preferentially extend pseudopods on matrices of higher stiffness (e.g., because of strain stiffening). In analogy to existing chemotaxis algorithms (46) at the time of copying we add the following durotaxis term to  $\Delta H$  in response to the strain- and orientation-dependent ECM stiffness  $E$ ,

$$\Delta H_{\text{durotaxis}} = -g(\vec{x}, \vec{x}') \lambda_{\text{durotaxis}} (f(E(\epsilon_1))(\vec{v}_1 \cdot \vec{v}_m)^2 + f(E(\epsilon_2))(\vec{v}_2 \cdot \vec{v}_m)^2), \quad (8)$$

with  $g(\vec{x}, \vec{x}') = 1$  for extensions and  $g(\vec{x}, \vec{x}') = -1$  for retractions,  $\lambda_{\text{durotaxis}}$  is a parameter,  $\vec{v}_m = \widehat{\vec{x} - \vec{x}'}$ , the copy direction, and  $\epsilon_1$  and  $\epsilon_2$ , and  $v_1$  and  $v_2$  eigenvalues and eigenvectors of  $\underline{\epsilon}$  representing the principal strains and strain orientation. The sigmoid  $f(E) = (1 + \exp(-\beta(E - E_\theta)))$  sets threshold stiffness  $E_\theta$ , and  $\beta$ , the steepness of the sigmoid. This function starts at zero, goes up when there is sufficient stiffness, and eventually reaches a maximum. This means that a certain level of stiffness is needed to cause a cell to spread. Due to limitations of our current finite element code and for reasons of computational efficiency, we assumed a linearly elastic, isotropic material in the FEM, thus precluding explicit strain stiffening effects in the FEM calculations. Instead, we implemented the effect of strain-stiffening in the cell response, where cells perceive increased ECM stiffness as a function of the local strain,

$$E(\epsilon) = E_0(1 + \epsilon/\epsilon_{\text{st}}), \quad (9)$$

where  $E_0$  sets a base stiffness for the substrate, and  $\epsilon_{\text{st}}$  is a stiffening parameter.

## Results

### Durotaxis

First we set out to capture, at a phenomenological level, the response of endothelial cells to static strains in the ECM in absence of cellular traction forces. When grown on statically, uniaxially strained collagen-enriched scaffolds, murine embryonic heart endothelial cells (H5V) cells orient in the direction of strain, whereas cells grown on unstrained scaffolds orient in random directions (47). Because the collagen fibers make the scaffold stiffen in the direction of strain, we hypothesized that the observed alignment of cells is due to durotaxis, the propensity of cells to migrate up gradients of substrate rigidity (48) and to spread on stiff substrates (49, 50). In our model we assumed (a) *strain stiffening*: a strained ECM is stiffer along the strain orientation than perpendicular to it, such that (b) due to durotaxis the endothelial cells preferentially extend pseudopods along the strain orientation, along which the ECM is stiffest, giving cells get

the most grip. To keep the finite-element problem computationally tractable, we assumed an isotropic and linearly elastic ECM. With these assumptions it is not possible to model strain stiffening explicitly. We therefore mimicked durotaxis by increasing the pseudopods’ probability of extension along the local strain orientation, and reducing the probability of retraction (see Methods for detail).

Fig. 2 *A* shows the response of the simulated cells to static stress. With increasing values of the durotaxis parameter  $\lambda_{\text{durotaxis}}$  (see Eq. 8, the endothelial cells elongate more. To test the sensitivity of the durotaxis method for lattice effects, we varied the orientation of the applied stress over a range  $[0 - 180]^\circ$  and measured the resulting orientation of the cells. Fig. 2 shows that the average orientation of the cells follows the orientation of the stretch isotropically. Thus the durotaxis component of our model phenomenologically reproduces published responses of endothelial cells to static stress (47).

## Cell traction

We next attempted to mimic the forces applied by cells onto the extracellular matrix, in absence of durotaxis. Traction-force microscopy experiments (31, 49) show that endothelial cells contract and exert tensional forces on the ECM. The forces are typically directed inward, towards the center of the cell, and forces concentrate at the tips of pseudopods. A recent modeling study (43) found that an accurate prediction of the direction and relative magnitudes of these traction forces within the cell can be obtained by assuming that each volume element  $i$  in the cell pulls on every other volume element in the cell  $j$  with a force proportional to their relative distance,  $d_{i,j}$ . Because this model gives experimentally plausible predictions for fibroblasts, endothelial cells and keratocytes (43), we adopted it to mimic the cell-shape dependent contractile forces that endothelial cells exert onto the ECM. Fig. 1 shows the contractile forces (*black*) and resulting ECM strains (*blue*) generated in our model by two adjacent cells. The traction forces and ECM strains become largest at the cellular “pseudopods”, qualitatively agreeing with traction force fields reported for endothelial cells (31).

## **Mechanical cell-ECM feedback qualitatively reproduces effect of substrate stiffness on cell shape**

The two previous sections discussed how the simulated cells can respond to and induce strain in the ECM in an experimentally plausible way. To test how the simulated cells respond to the strains they generate themselves, we studied the behavior of simulated, single cells in presence of both the durotaxis and the cell traction mechanisms. As Fig. 3 and Movie S1 demonstrate, matrix stiffness affects both the morphology and motility of the simulated cells. On the most compliant substrate tested (0.5 kPa) the simulated cells contract and round up, whereas cells spread isotropically on the stiffest substrate tested (32 kPa). On matrices of intermediate stiffnesses (around 12 kPa) cells elongate. Such dependence of cellular morphology on the stiffness of the ECM mimics the behavior of endothelial cells (49) and cardiac myocytes (33) in matrices of diverse stiffness. Thus the model rules for cell traction and stretch guidance based on durotaxis and strain stiffening suffice to reproduce an experimentally plausible cellular response to matrix stiffness.

## **Mechanical cell-ECM feedback coordinates behavior of adjacent cells**

Reinhart-King and co-workers (2) demonstrated that strains induced by endothelial cells on a compliant substrate can affect the behavior of adjacent cells (2). On soft substrates (5.5 kPa or below) the cells reduced the motility of adjacent cells, whereas on stiff substrates (33 kPa) such an effect was not found. On substrates of intermediate stiffness (5.5 kPa), adjacent endothelial cells repeatedly attached and detached from one another. They also showed that on 5.5kPa substrates cells move more slowly in close vicinity of other cells, than when they are on their own. Because the extent to which cells could affect the motility of nearby cells depended on matrix compliancy, Reinhart-King et al.(2) proposed that mechanical traction forces could act as a means for cell-cell communication. To test if the simple strain-based mechanism represented in our model suffices for reproducing such mechanical cell-cell communication, we initiated the simulations with pairs of cells placed adjacent to one another at a distance of fourteen lattice

sites corresponding with a distance of  $3.5 \mu\text{m}$ , and ran a series of simulations on substrates of varying stiffness (Fig. 4 *A* and Movie S2). The cells behaved similar to the single cell simulations (Fig. 3), with little cell-cell interactions at the lower and higher stiffness ranges. Consistent with the observations by Reinhart-King (2), cell pairs on substrates of intermediate stiffness (12-14 kPa) dispersed more slowly than individual cells, whereas individual cells and cell pairs dispersed at identical rates on stiff (16 kPa or more) or soft (below 10 kPa) substrates (Fig. 4, *B-D*). Also in agreement with the observations of Reinhart-King et al. (2), on a simulated substrate of intermediate stiffness (12 kPa) the cells responded to the matrix strains induced by the adjacent cell by repeatedly touching each other, and separating again (Fig. 4 *E*).

Mechanical strain can also coordinate the orientation of cells. Fibroblasts seeded on a compliant gel tend to align in a nose-to-tail fashion along the orientation of mechanical strain (51). Bishofs and Swartz (40) proposed a computational model to explain this observation. Their model assumes that cells prefer the direction of maximal effective stiffness, where the cell has to do the least work to build up a force. This work is minimal between two aligned cells, because maximum strain stiffening occurs along the axis of contraction. Interestingly, visualization of our model results (Fig. 2 *C*) suggested similar nose-to-tail alignment of our model cells at around 12 kPa. To quantify such alignment in our simulations, we measured the angle  $\alpha$  between the lines  $l_1$  and  $l_2$ , defining the long axes of the cells and crossing the centers of mass as the cells (Fig. 4 *F*). We classified the angles as acute ( $\alpha < \pi/2$ ; *i.e.* no alignment) or obtuse ( $\alpha \geq \pi/2$ ; alignment). At matrix stiffnesses up to around 10 kPa, about half of the angles  $\alpha$  were obtuse, corresponding with the expected value for uncorrelated cell orientations. However, at 12 kPa and 14 kPa significantly more than half of the cell pairs had oriented into obtuse triangles (78/100 for 12 kPa,  $p = 7.95 \times 10^{-9}$  and 72/100 for 14 kPa,  $p = 6.29 \times 10^{-6}$ , binomial test), suggesting that the mechanical coupling represented in our model causes cells to align in a head-to-tail fashion.

## Mechanical cell-cell communication drives biologically-realistic collective cell behavior

After observing that the local, mechanical cell-ECM interaction assumed in our model sufficed for correctly reproducing many aspects of the behavior of individual endothelial cells on compliant matrices and of the mechanical communication of pairs of endothelial cells on compliant matrices, we asked what collective cell behavior the mechanical cell-cell coordination produced. When seeded subconfluently onto a compliant matrix (e.g., Matrigel), endothelial cells tend to organize into polygonal, vascular-like networks (5, 52, 6, 53). To mimic such endothelial cell cultures, we initialized our simulations with 450 cells uniformly distributed over a lattice of  $300 \times 300$  pixels ( $0.75 \times 0.75 \text{ mm}^2$ ), corresponding with a cell density of 800 endothelial cells per  $\text{mm}^2$ . In accordance with experimental observations (6), after 3000 MCS networks had not formed on soft matrices (0.5-4 kPa) or on stiff matrices (16-32 kPa) (Fig. 5 A): the cells tended to form small clusters (Fig. 5 A). Interestingly, on matrices of intermediate stiffness after around 300 MCS the cells organized into chains (8 kPa) or network-like structures (10 kPa and 12 kPa) similar to vascular network-like structures observed in endothelial cell cultures (5, 52, 6, 53).

Fig. 5 B and Movie S3 show a time-lapse of the development of a network configuration on a substrate of 10kPa. The cells organize into a network structure with a few hundred Monte Carlo steps. The networks stay dynamically stable, with minor remodeling events taking place, including closure and splitting of lacunae. Fig. 5 C shows such a splitting event in detail. In an existing lacuna ( $t=1800$ ) stretch lines bridge the lacunae, and connect two groups of cells penetrating the lacuna ( $t=1980$ ). The cells preferentially follow the path formed by these stretch lines ( $t=2150$ ) and have reached the other side of the lacuna by  $t=2400$ . Interestingly, similar bridging events were observed in endothelial cell cultures (6).

We next asked if the mechanical model could also reproduce sprouting from endothelial spheroids (7, 8). Fig. 6 shows the results of simulations initiated with a two-dimensional spheroid of cells after 3000 MCS. On soft (0.5-8 kPa) and on stiff (32 kPa) matrices the spheroids stayed intact over the time course of the simulation. On intermediary stiffnesses (10-12 kPa) the

spheroids formed distinct sprouts, visually resembling the formation of sprouts in in vitro endothelial spheroids (7, 8). On the 14 kPa and 16 kPa matrices the cells migrated away from the spheroid, with some cell alignment still visible for the 14 kPa matrices. Observation of a sprout protruding from a spheroid at 10 kPa suggests that a new sprout starts when one of the cells at the edge of the cluster protrudes and increases the strain in front of it. In a positive feedback loop this strain, via an increase in perceived stiffness, guides the protruding cell forward. The strain in its wake then guides the other cells along (Fig. 6 *C*).

## Discussion

In this paper we introduced a novel computational model of the in vitro collective behavior of endothelial cells seeded on compliant substrates. The model is based on the experimentally plausible assumptions that (a) endothelial cells generate mechanical strains in the substrate (43, 31), (b) they perceive a stiffening of the substrate along the strain orientation, and (c) they extend preferentially on stiffer substrate.(47). Thus, in short, the assumptions are: cell traction, strain stiffening, and durotaxis. The model simulations showed that these assumptions suffice to reproduce, in silico, experimentally observed behavior of endothelial cells at three higher-level, spatial scales: the single cell level, cell pairs, and the collective behavior of endothelial cells. In accordance with experimental observation (49, 33), the simulated cells spread out on stiff matrices, they contracted on soft matrices, and elongate on matrices of intermediate stiffness (Fig. 3). The same assumptions also suffice to reproduce experimentally observed pairwise cell-cell coordination. On matrices of intermediate stiffness, endothelial cells slow down each other (Fig. 4 *B*) and repeatedly touch and retract from each other (Fig. 4 *E* and Movie S2), in agreement with in vitro observations of bovine aortic endothelial cells on acrylamide gels (2). Also, in agreement with experimental observations of fibroblasts on compliant substrates (51) and previous model studies (40) the cells repositioned into an aligned, head-to-tail orientation (Fig. 4 *F*). The model simulation further suggest that these pairwise cell-cell interactions suffice for vascular-like network formation in vitro (Fig. 5 and sprouting of endothelial spheroids (Fig. 6).

The correlation between pairwise cell-cell interactions and collective cell behavior observed in our computational model parallels observations *in vitro*. Cells elongate due to positive feedback between stretch-guided extension and cell traction, as previously suggested by Winer et al. (54). Elongated and spindle-shaped cells are considered indicative of future cell network assembly (6). Our model suggests that the elongated cell shapes produce oriented strains in the matrix, via which cells sense one another at a distance. In this way new connections are continuously formed over “strain bridges” (see e.g. Fig. 5 *C*), while other cellular connections break producing dynamically stable networks as illustrated in Movie S3. Such dynamic network restructuring was also observed during early embryonic development of the quail embryo (55) and in bovine aortic endothelial cell cultures (6), but not in human umbilical vein endothelial cell cultures (21, 53). Also in agreement with experimental results, the collective behavior predicted by our model strongly depends on substrate stiffness. The strongest interaction between cell pairs is found on substrates of intermediate stiffness, enabling network formation (2), whereas network assembly cannot occur stiff substrates(6).

These agreements with experimental results are encouraging, but our model also lacks a number of properties of *in vitro* angiogenesis that pinpoint key components still missing from our description. In our simulations, single cells dispersed more quickly on soft gels (Fig. 4 *B*) than on stiff gels (Fig. 4 *D* and Fig. S1). This model behavior contradicts experimental observations showing that endothelial cells move fastest on stiff substrates (2). Also, although the model correctly predicts the absence of network formation on stiff substrates, it cannot yet explain the observation that reducing the substrate adhesivity of the endothelial cells rescues network formation (6). On compliant gels endothelial cells must secrete fibronectin to form stable networks, whereas fibronectin polymerization inhibitors elicit spindle-like cellular phenotypes associated with network formation on stiff matrices, under conditions where networks do not normally form (6). To explain these observations, straightforward future extensions of the model will include a more detailed description of cell-substrate adhesion, combined with models of ECM secretion and proteolysis (23, 13, 56, 24).

The current model also assumes a uniform density and thickness of the extracellular matrix, whereas under some culture conditions the endothelial cells have been reported to pull the extracellular matrix underneath them (57), producing gradient in matrix density and/or thickness. Manoussaki et al. (15) and Namy et al.(17) showed that such matrix pulling may mediate attractive forces between the endothelial cells and drive formation of networks, either due to passive cell movement along with the matrix (15) or haptotaxis along the ECM density gradients. These models (15, 17) included an anisotropic diffusion term to simulate preferential movement along the local strain-direction, but the term was neither necessary nor sufficient for network formation. This finding contradicts our model in which strain-induced sprouting is the driving force of network formation and sprouting. Possibly the two models represent the two extremes of network formation on visco-elastic matrices. Here, the Manoussaki et al. and Namy et al. models represent patterning on viscous matrices, in which cellular traction forces pull the matrix together while inducing little strain or stress. Our model would represent elastic materials, in which pulling forces induce local strains. Future extensions of the model will include matrix flows (e.g. by assuming a matrix thickness field) allowing us to study the full range of viscoelastic matrices.

Apart from these biological issues, we made several mathematical simplifications that we will improve upon in future models of cell-ECM interactions. In the current model, for computational efficiency, we used a finite element model with linearly elastic materials, and mimicked durotaxis via a perceived strain-stiffening (Eq. 9) where cells perceive increased ECM stiffness due to local strain. In our ongoing work we are interfacing the open source package FEBio (<http://febio.org>) with the Cellular Potts package CompuCell3D (<http://compuCell3d.org>). This will allow us to run our model with any ECM material available to users of FEBio, including strain-stiffening materials. Using an actual strain stiffening material may lead to longer-range interactions between cells, because locally stiffer regions may channel the stress between the cells (58). A further technical limitation of our model is that we currently only run two-dimensional simulations, representing cells moving on top of a two-dimensional culture system. The ongoing

interfacing of FEBio and CompuCell3D will pave the way for modeling cell-ECM interactions in three-dimensional tissue cultures.

A quite puzzling aspect of vascular network formation and spheroid sprouting is that so many alternative, often equally plausible computational models can explain it (reviewed in (12)). Including the present model, there are at least three alternative computational models based on mechanical cell-ECM interactions (15, 28, 16, 17, 59), a series of models assuming chemoattraction between endothelial cells (18, 19, 60, 21, 22, 61) and extensions thereof (62, 23, 24), and models explaining network formation in absence of chemical or mechanical fields (26, 29, 27). Each of the models explain one aspect of vascular network formation or a response to an experimental treatment that the other models cannot explain, e.g. the relation between spindle shaped cell phenotypes and network formation (21, 27) for models, the requirement of VE-cadherin signaling for network formation and sprouting (22, 26), the binding and release of growth factors from the ECM (23), the role of mechanical ECM restructuring and haptotaxis (15, 28, 17), the response of vascular networks to toxins (24), or the role of intracellular  $\text{Ca}^{2+}$  signaling (62). Among these alternative models, we must now experimentally falsify incorrect mechanisms, and fine-tune and possibly combine the remaining models to arrive at a more complete understanding of the mechanisms of angiogenesis. To this end, we are currently quantitatively comparing the kinetics of patterns produced by chemotaxis-based, traction-based, and cell-elongation based models with the kinetics of in vitro networks (21, 53). There resulting, more complete model would likely contain aspects of each the available computational models and assist in explained the conflicting results obtained from the available experimental systems, culture conditions, and in silico models of angiogenesis.

## Acknowledgments

The authors thank Sonja Boas for critical reading of the manuscript.

The investigations were supported by the Division for Earth and Life Sciences (ALW) with financial aid from the Netherlands Organization for Scientific Research (NWO). This work was

cofinanced by the Netherlands Consortium for Systems Biology (NCSB) which is part of the Netherlands Genomics Initiative / Netherlands organization for Scientific Research.

## Supporting Material

The supporting Material includes a supporting table, a supporting figure, four supporting videos, the simulation code and documentation of the simulation code.

## Supporting citations

Reference (63) appears in the Supporting Material.

## References

1. Hynes, R. O., 2009. The extracellular matrix: not just pretty fibrils. *Science* 326:1216–1219.
2. Reinhart-King, C. A., Dembo, M., and Hammer, D. A., 2008. Cell-cell mechanical communication through compliant substrates. *Biophys. J.* 95:6044–6051.
3. Mammoto, A., Connor, K. M., Mammoto, T., Yung, C. W., Huh, D., Aderman, C. M., Mostoslavsky, G., Smith, L. E. H., and Ingber, D. E., 2009. A mechanosensitive transcriptional mechanism that controls angiogenesis. *Nature* 457:1103–1108.
4. Nelson, C. M., Jean, R. P., Tan, J. L., Liu, W. F., Sniadecki, N. J., Spector, A. A., and Chen, C. S., 2005. Emergent patterns of growth controlled by multicellular form and mechanics. *P. Natl. Acad. Sci. USA* 102:11594–11599.
5. Folkman, J. and Hauenschild, C., 1980. Angiogenesis in vitro. *Nature* 288:551–556.
6. Califano, J. and Reinhart-King, C., 2008. A balance of substrate mechanics and matrix chemistry regulates endothelial cell network assembly. *Cell Mol. Bioeng.* 1:122–132.

7. Korff, T. and Augustin, H. G., 1999. Tensional forces in fibrillar extracellular matrices control directional capillary sprouting. *J. Cell Sci.* 112:3249–3258.
8. Kniazeva, E. and Putnam, A. J., 2009. Endothelial cell traction and ECM density influence both capillary morphogenesis and maintenance in 3-D. *Am. J. Physiol.-Cell Ph.* 297:C179–C187.
9. Vernon, R. B. and Sage, E. H., 1995. Between molecules and morphology. Extracellular matrix and creation of vascular form. *Am. J. Pathol.* 147:873–883.
10. Vernon, R. B. R., Lara, S. L. S., Drake, C. J. C., Iruela-Arispe, M. L. M., Angello, J. C. J., Little, C. D. C., Wight, T. N. T., and Sage, E. H. E., 1995. Organized type I collagen influences endothelial patterns during "spontaneous angiogenesis in vitro": planar cultures as models of vascular development. *In Vitro Cell Dev.-An.* 31:120–131.
11. Koolwijk, P., van Erck, M. G., de Vree, W. J., Vermeer, M. A., Weich, H. A., Hanemaaijer, R., and van Hinsbergh, V. W., 1996. Cooperative effect of  $\text{TNF}\alpha$ , bFGF, and VEGF on the formation of tubular structures of human microvascular endothelial cells in a fibrin matrix. Role of urokinase activity. *J. Cell Biol.* 132:1177–1188.
12. Merks, R. M. H. and Koolwijk, P., 2009. Modeling morphogenesis in silico and in vitro: Towards quantitative, predictive, cell-based modeling. *Math. Model. Nat. Pheno.* 4:149–171.
13. Boas, S. E. M., Palm, M. M., Koolwijk, P., and Merks, R. M. H., 2012. Computational modeling of angiogenesis: Towards a multi-scale understanding of cell–cell and cell–matrix interactions. In *Mechanical and Chemical Signaling in Angiogenesis*, 161–183. Springer Berlin Heidelberg, Berlin, Heidelberg.
14. Scianna, M., Bell, C. G., and Preziosi, L., 2013. A review of mathematical models for the formation of vascular networks. *J. Theor. Biol.* 333:174–209.

15. Manoussaki, D., Lubkin, S., Vernon, R., and Murray, J., 1996. A mechanical model for the formation of vascular networks in vitro. *Acta Biotheor.* 44:271–282.
16. Manoussaki, D., 2003. A mechanochemical model of angiogenesis and vasculogenesis. *ESAIM: Math. Model. Num.* 37:581–599.
17. Namy, P., Ohayon, J., and Tracqui, P., 2004. Critical conditions for pattern formation and in vitro tubulogenesis driven by cellular traction fields. *J. Theor. Biol.* 227:103–120.
18. Gamba, A., Ambrosi, D., Coniglio, A., de Candia, A., Di Talia, S., Giraudo, E., Serini, G., Preziosi, L., and Bussolino, F., 2003. Percolation, morphogenesis, and Burgers dynamics in blood vessels formation. *Phys. Rev. Lett.* 90:118101.
19. Serini, G., Ambrosi, D., Giraudo, E., Gamba, A., Preziosi, L., and Bussolino, F., 2003. Modeling the early stages of vascular network assembly. *EMBO J.* 22:1771–1779.
20. Keller, E. F. and Segel, L. A., 1970. Initiation of slime mold aggregation viewed as an instability. *J. Theor. Biol.* 26:399–415.
21. Merks, R. M. H., Brodsky, S. V., Goligorsky, M. S., Newman, S. A., and Glazier, J. A., 2006. Cell elongation is key to in silico replication of in vitro vasculogenesis and subsequent remodeling. *Dev. Biol.* 289:44–54.
22. Merks, R. M. H., Perryn, E. D., Shirinifard, A., and Glazier, J. A., 2008. Contact-inhibited chemotaxis in de novo and sprouting blood-vessel growth. *PLoS Comp Biol* 4:e1000163.
23. Köhn-Luque, A., De Back, W., Starruß, J., Mattiotti, A., Deutsch, A., Pérez-Pomares, J. M., and Herrero, M. A., 2011. Early embryonic vascular patterning by matrix-mediated paracrine signalling: A mathematical model study. *PLoS ONE* 6:e24175.
24. Kleinstreuer, N., Dix, D., Rountree, M., Baker, N., Sipes, N., Reif, D., Spencer, R., and Knudsen, T., 2013. A computational model predicting disruption of blood vessel development. *PLoS Comput. Biol.* 9:e1002996.

25. Singh, J., Hussain, F., and Decuzzi, P., 2013. Role of differential adhesion in cell cluster evolution: for vasculogenesis to cancer metastasis. *Comput. Method. Biomec.* .
26. Szabó, A., Perryn, E. D., and Czirok, A., 2007. Network formation of tissue cells via preferential attraction to elongated structures. *Phys. Rev. Lett.* 98:038102.
27. Palm, M. M. and Merks, R. M. H., 2013. Vascular networks due to dynamically arrested crystalline ordering of elongated cells. *Phys. Rev. E* 87:012725.
28. Murray, J. D., Manoussaki, D., Lubkin, S. R., and Vernon, R. B., 1996. A mechanical theory of in vitro vascular network formation. In V. A. Mironov, C. Little, and H. Sage, editors, *Vascular morphogenesis: in vivo, in vitro, in mente*, 173–188. Birkhäuser, Boston.
29. Szabó, A., Mehes, E., Kosa, E., and Czirok, A., 2008. Multicellular sprouting in vitro. *Biophys. J.* 95:2702–2710.
30. Tan, J. L., Tien, J., Pirone, D. M., Gray, D. S., Bhadriraju, K., and Chen, C. S., 2003. Cells lying on a bed of microneedles: an approach to isolate mechanical force. *P. Natl. Acad. Sci. USA* 100:1484–1489.
31. Reinhart-King, C. A., Dembo, M., and Hammer, D. A., 2005. The dynamics and mechanics of endothelial cell spreading. *Biophys. J.* 89:676–689.
32. Califano, J. P. and Reinhart-King, C. A., 2010. Exogenous and endogenous force regulation of endothelial cell behavior. *J. Biomech.* 43:79–86.
33. Winer, J. P., Chopra, A., Kresh, J. Y., and Janmey, P. A., 2011. Substrate elasticity as a probe to measure mechanosensing at cell-cell and cell-matrix junctions. In W. JA and H. BAC, editors, *Mechanobiology of Cell-Cell and Cell-Matrix Interactions*, 11–22. Springer US, Boston, MA.
34. Graner, F. and Glazier, J. A., 1992. Simulation of biological cell sorting using a two-dimensional extended Potts model. *Phys. Rev. Lett.* 69:2013–2016.

35. Glazier, J. A. and Graner, F., 1993. Simulation of the differential adhesion driven rearrangement of biological cells. *Phys. Rev. E* 47:2128–2154.
36. Huebner, K. H., Dewhurst, D. L., Smith, D. E., and Byrom, T. G., 1975. The finite element method for engineers. John Wiley & Sons, London.
37. Davies, A. J., 1980. The finite element method: a first approach. Clarendon Press, Oxford.
38. Davies, A. J., 2011. The finite element method: An introduction with partial differential equations. Oxford University Press, Oxford.
39. Ambrosi, D., 2006. Cellular traction as an inverse problem. *Siam J Appl Math* 66:2049–2060.
40. Bischofs, I. B. and Schwarz, U. S., 2003. Cell organization in soft media due to active mechanosensing. *P. Natl. Acad. Sci. USA* 100:9274–9279.
41. Soofi, S. S., Last, J. A., Liliensiek, S. J., Nealey, P. F., and Murphy, C. J., 2009. The elastic modulus of Matrigel<sup>TM</sup> as determined by atomic force microscopy. *J. Struct. Biol.* 167:216–219.
42. Boudou, T., Ohayon, J., Picart, C., and Tracqui, P., 2006. An extended relationship for the characterization of Young’s modulus and Poisson’s ratio of tunable polyacrylamide gels. *Biorheology* 43:721–728.
43. Lemmon, C. A. and Romer, L. H., 2010. A predictive model of cell traction forces based on cell geometry. *Biophys. J.* 99:L78–L80.
44. Aratyn-Schaus, Y., Oakes, P. W., and Gardel, M. L., 2011. Dynamic and structural signatures of lamellar actomyosin force generation. *Mol. Biol. Cell.* 22:1330–1339.
45. Strang, G., 1986. Introduction to applied mathematics. Wellesley-Cambridge Press, Wellesley, MA.

46. Savill, N. and Hogeweg, P., 1997. Modelling morphogenesis: From single cells to crawling slugs. *J. Theor. Biol.* 184:229–235.
47. van der Schaft, D. W. J., van Spreeuwel, A. C. C., Van Assen, H. C., and Baaijens, F. P. T., 2011. Mechanoregulation of vascularization in aligned tissue-engineered muscle: A role for vascular endothelial growth factor. *Tissue Eng. Pt. A* 17:2857–2865.
48. Lo, C.-M., Wang, H.-B., Dembo, M., and Wang, Y.-L., 2000. Cell movement Is guided by the rigidity of the substrate. *Biophys. J.* 79:144–152.
49. Califano, J. P. and Reinhart-King, C. A., 2010. Substrate stiffness and cell area predict cellular traction stresses in single cells and cells in contact. *Cell Mol. Bioeng.* 3:68–75.
50. Pelham, R. J. R. and Wang, Y. I. Y., 1997. Cell locomotion and focal adhesions are regulated by substrate flexibility. *P. Natl. Acad. Sci. USA* 94:13661–13665.
51. Takakuda, K. and Miyairi, H., 1996. Tensile behaviour of fibroblasts cultured in collagen gel. *Biomaterials* 17:1393–1397.
52. Kubota, Y., Kleinman, H. K., Martin, G. R., and Lawley, T. J., 1988. Role of laminin and basement membrane in the morphological differentiation of human endothelial cells into capillary-like structures. *J. Cell Biol.* 107:1589–1598.
53. Parsa, H., Upadhyay, R., and Sia, S. K., 2011. Uncovering the behaviors of individual cells within a multicellular microvascular community. *P. Natl. Acad. Sci. USA* 108:5133–5138.
54. Winer, J. P., Oake, S., and Janmey, P. A., 2009. Non-linear elasticity of extracellular matrices enables contractile cells to communicate local position and orientation. *PLoS ONE* 4:e6382.
55. Rupp, P. A., Czirók, A., and Little, C. D., 2004.  $\alpha v\beta 3$  integrin-dependent endothelial cell dynamics in vivo. *Development* 131:2887–2897.

56. Daub, J. T. and Merks, R. M. H., 2013. A cell-based model of extracellular-matrix-guided endothelial cell migration during angiogenesis. *B. Math. Biol.* 1–23.
57. Vernon, R. B., Angello, J. C., Iruelaarispe, M. L., Lane, T. F., and Sage, E. H., 1992. Reorganization of basement-membrane matrices by cellular traction promotes the formation of cellular networks invitro. *Lab. Invest.* 66:536–547.
58. Rudnicki, M. S. and Billiar, K. L., 2011. Effective stiffness of thin nonlinear gel substrates. In *IEEE -2011 37th Annual Northeast Bioengineering Conference (NEBEC)*, 1–2.
59. Tranqui, L. and Tracqui, P., 2000. Mechanical signalling and angiogenesis. The integration of cell-extracellular matrix couplings. *C.R. Acad. Sci. III-Vie* 323:31–47.
60. Merks, R. M. H., Newman, S. A., and Glazier, J. A., 2004. Cell-oriented modeling of In vitro capillary development. *Lect. Notes Comput. Sci.* 3305:425–434.
61. Guidolin, D., Albertin, G., Sorato, E., Oselladore, B., Mascarin, A., and Ribatti, D., 2009. Mathematical modeling of the capillary-like pattern generated by adrenomedullin-treated human vascular endothelial cells in vitro. *Dev. Dyn.* 238:1951–1963.
62. Scianna, M., Munaron, L., and Preziosi, L., 2011. A multiscale hybrid approach for vasculogenesis and related potential blocking therapies. *Prog. Biophys. Mol. Bio.* 106:450–462.
63. Baaijens, F., 2004. Numerical analysis of continua - lecture notes. Technical Report 4798, Eindhoven University of Technology, Eindhoven.

## Figure Legends

FIGURE 1. Visualization of simulated traction forces (*black arrows*) and resulting matrix strains (*blue line segments*) generated in the proposed hybrid Cellular Potts and finite-element model

FIGURE 2. Simulated cellular responses to static strains. Cells do not generate traction forces in this figure. (A) Cell length as a function of the guidance parameter on a substrate stretched along the vertical axis. (B) Cell orientation as a function of the strain orientation.  $\alpha=10$  (simulated with  $\alpha=10$ ). Error bars show standard deviation for  $n = 100$ . Insets show five simulations per value tested

FIGURE 3. (A) Single cells on substrates of varying stiffnesses after 100 MCS. (B) Cell length as a function of substrate stiffness. (C) Cell eccentricity as a function of cell length

FIGURE 4. Simulated cell-cell interactions on substrates of varying stiffnesses. (A) Visualization of cell shapes and substrate strains in absence of external strain. Line pieces indicate strain magnitude and orientation. (B-D) Mean square displacement of individual cells (*blue errorbars*) and cell pairs (*red errorbars*) on simulated substrates. (B) 4 kPa; (C) 12 kPa; (D) 32 kPa. Error bars indicate standard deviation for  $n = 100$  after 500 MCS. (E) Number of cell-cell contacts made over 500 MCS between two simulated cells initiated at a distance of fourteen lattice sites from each other. (F) Quantification of head-to-tail alignment of cells. An obtuse angle between the two cells' long axes indicates that cells are oriented head-to-tail. Plotted is the fraction of Monte Carlo steps that the two cells are aligned head-to-tail, over 100 independent simulations of 500 MCS on a field of  $0.25 \times 0.25 \text{ mm}^2$  ( $100 \times 100$  pixels). Measurements start from 20 MCS

FIGURE 5. Simulated network formation assay. (A) Simulated collective cell behavior on substrates of varying stiffness, with a uniformly distributed initiated configuration of cells. (B) Time lapse showing the development of a polygonal network on a 10kPa substrate (time in MCS). Panels A and B represent a  $0.75 \times 0.75 \text{ mm}^2$  area ( $300 \times 300$  pixels) initiated with 450 cells. (C) Close-up of simulated network formation on a 10 kPa substrate, showing the reconnection of two sprouts. Time in MCS. (D) Sprouting observed in cultures of bovine aortic endothelial cells, where circled regions highlight endothelial cells sprouting from existing cords. Time in hours. Bar =  $50 \mu\text{m}$ . Panel D reproduced from (6) with permission.

FIGURE 6. Simulated spheroid assay. (A) Collective behavior in a simulation initiated with a

two-dimensional “spheroid” of cells, on substrates of varying stiffness. (*B*) Time lapse showing a sprouting spheroid on a 10kPa substrate. Time in MCS. Panels *A* and *B* represent a  $0.75 \times 0.75 \text{ mm}^2$  area ( $300 \times 300$  pixels) initiated with a spheroid consisting of 113 cells; (*C*) Close-up of sprouting on a 10 kPa substrate. Time in MCS. Black line pieces indicate strain magnitude and orientation

# Figures

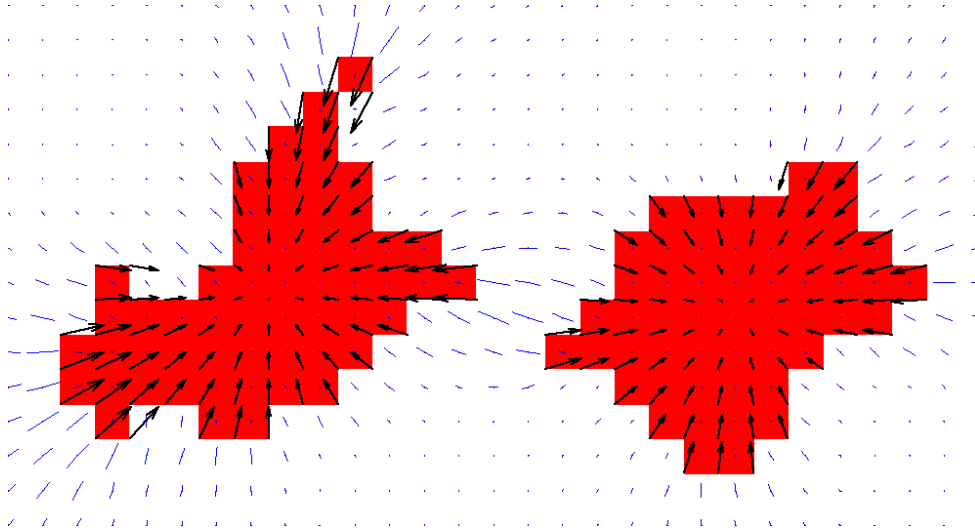


Figure 1

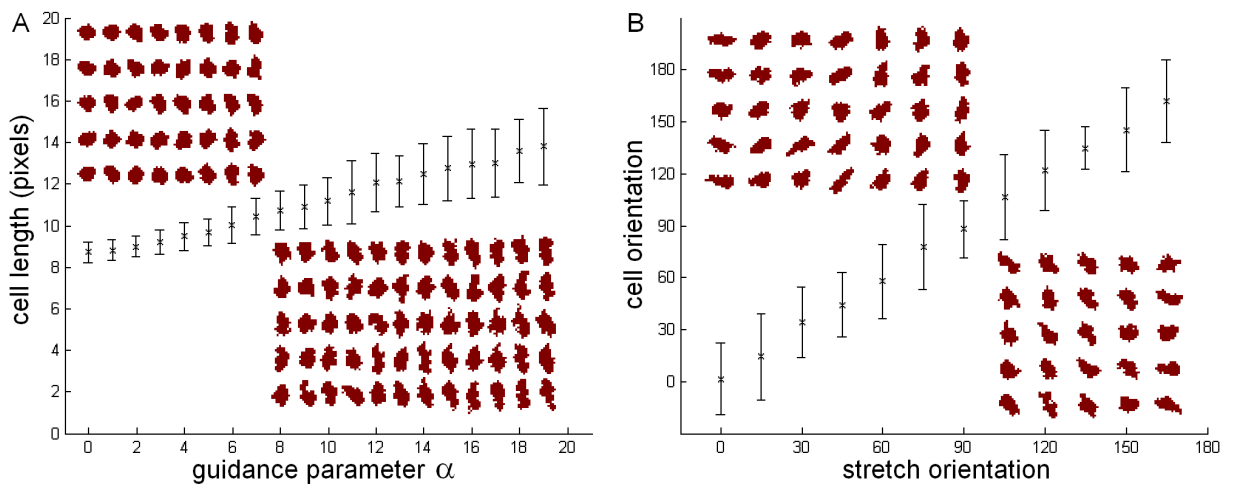
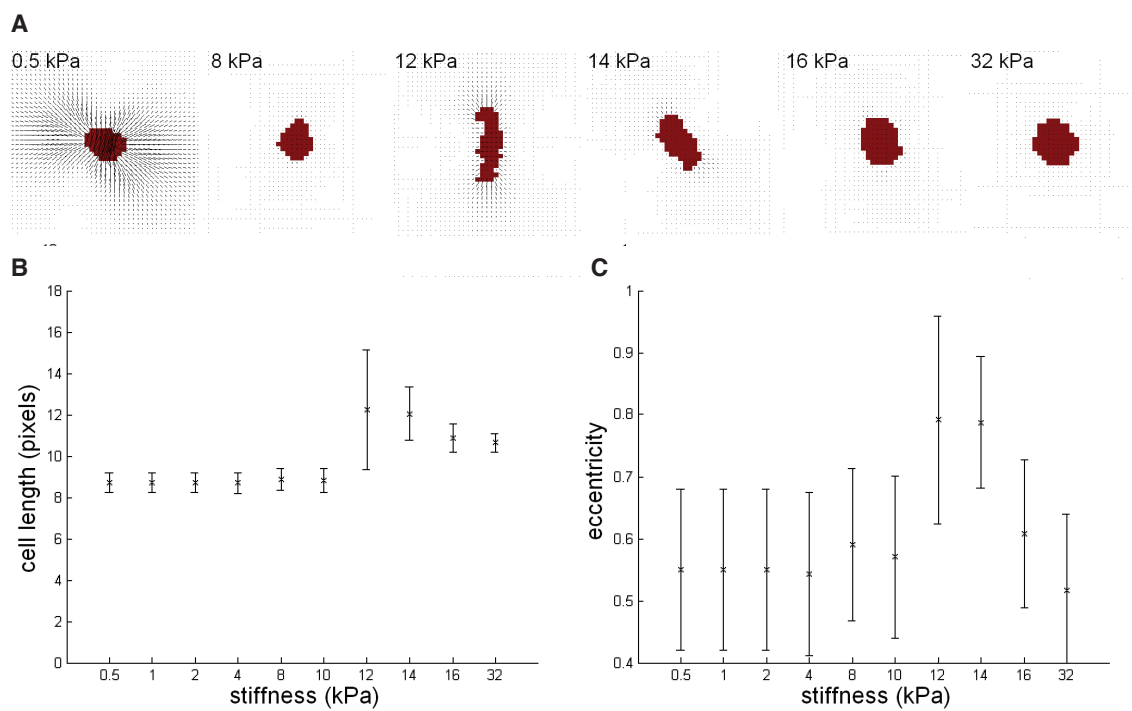


Figure 2



**Figure 3**

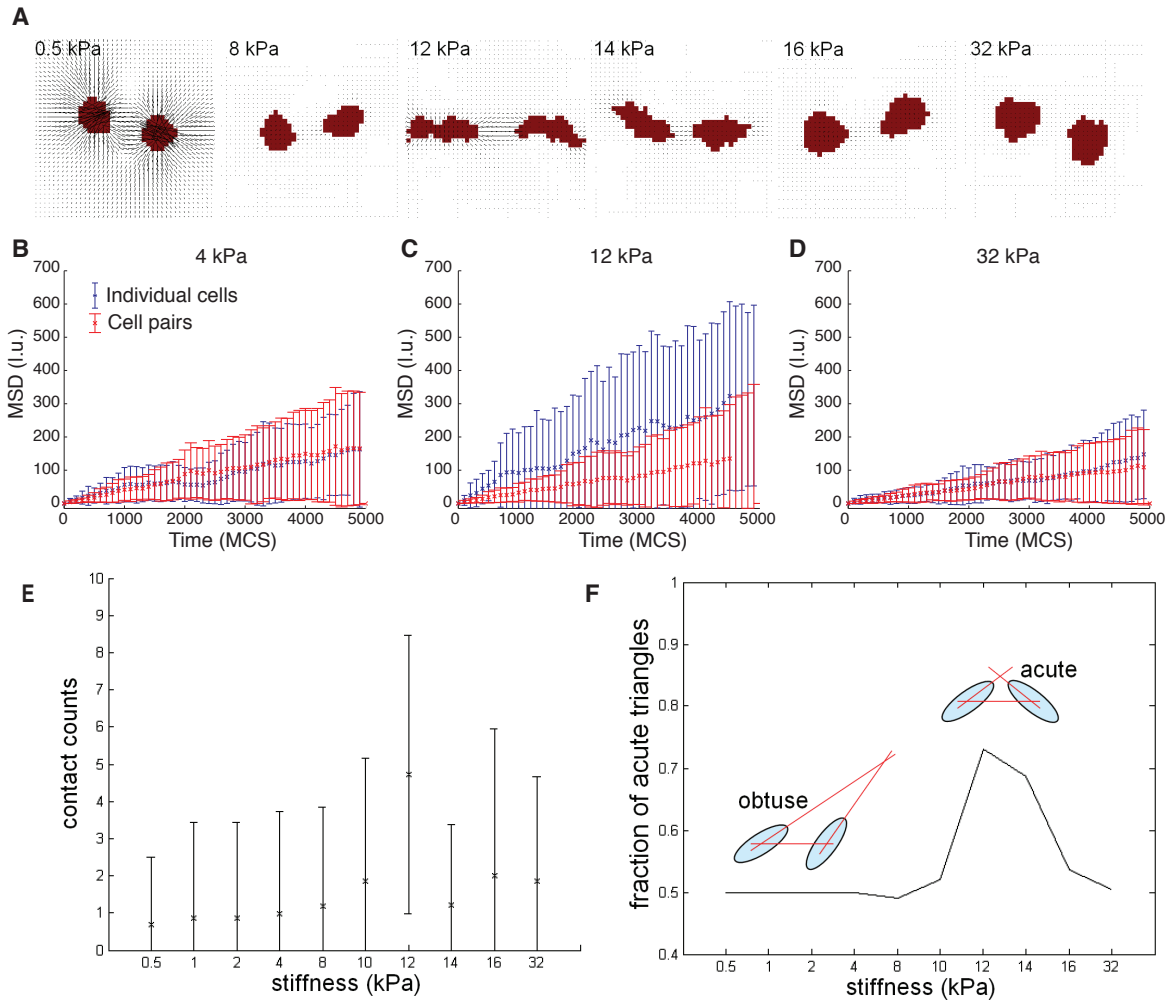


Figure 4

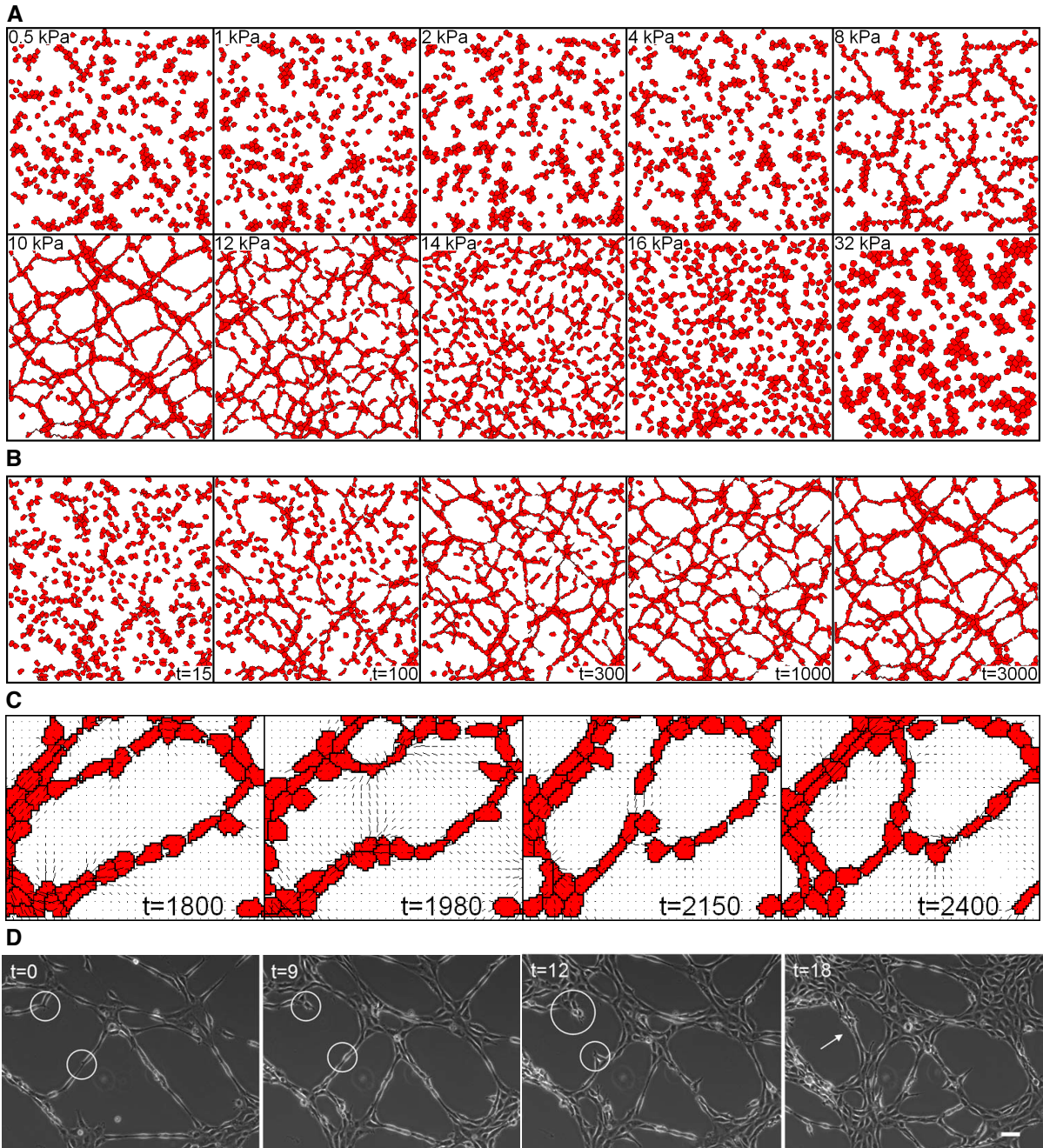


Figure 5

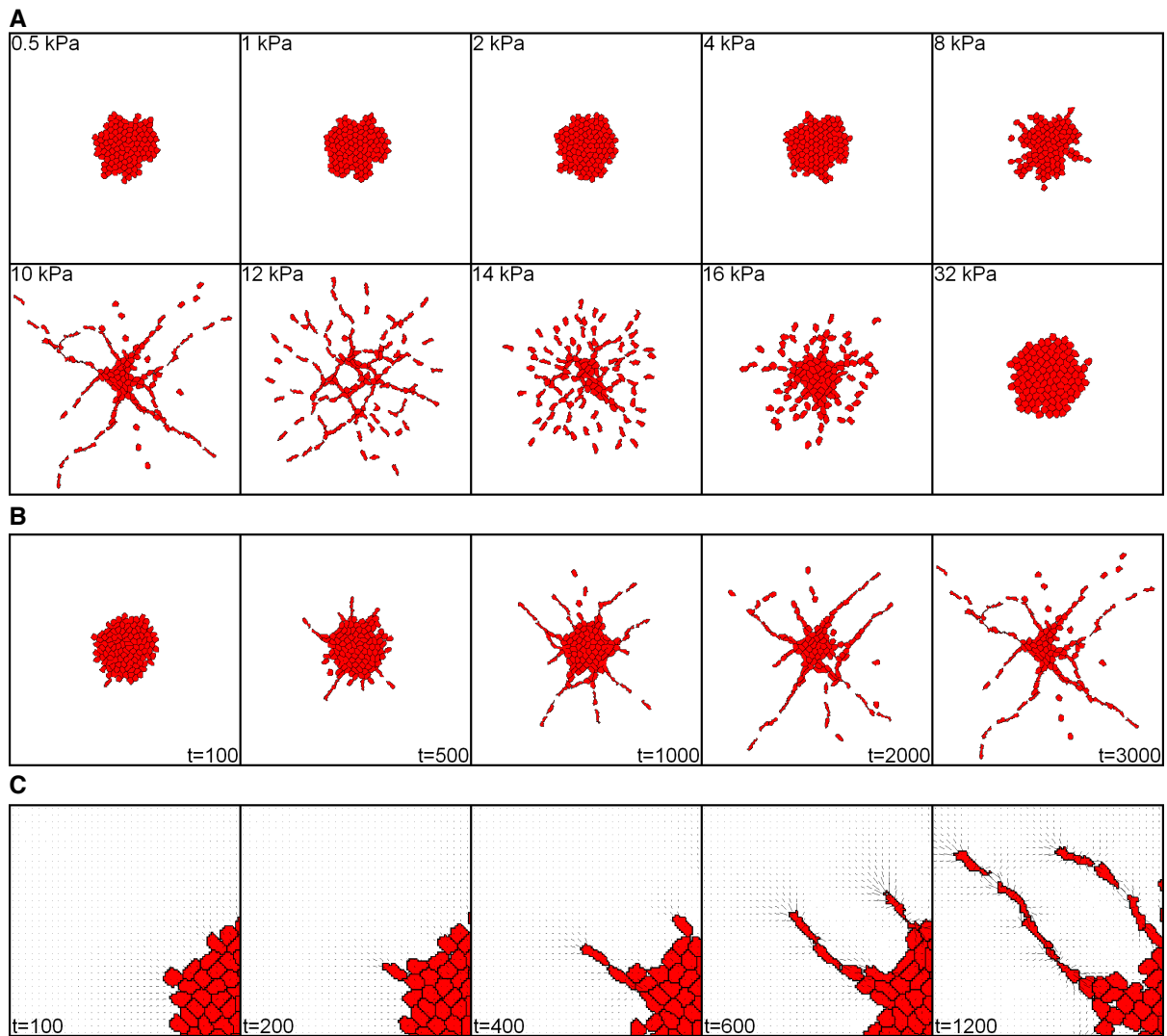


Figure 6